Published OnlineFirst June 30, 2020; DOI: 10.1158/0008-5472.CAN-19-2745

CXCR4 in Tumor Epithelial Cells Mediates Desmoplastic Reaction in Pancreatic Ductal Adenocarcinoma

Toshihiro Morita[1], Yuzo Kodama[1,2], Masahiro Shiokawa[1], Katsutoshi Kuriyama[1], Saiko Marui[1], Takeshi Kuwada[1], Yuko Sogabe[1], Tomoaki Matsumori[1], Nobuyuki Kakiuchi[1], Teruko Tomono[1], Atsushi Mima[1], Tatsuki Ueda[1], Motoyuki Tsuda[1], Yuki Yamauchi[1], Yoshihiro Nishikawa[1], Yojiro Sakuma[1], Yuji Ota[1], Takahisa Maruno[1], Norimitsu Uza[1], Takashi Nagasawa[3], Tsutomu Chiba[1,4], and Hiroshi Seno[1]

ABSTRACT

Pancreatic ductal adenocarcinoma (PDAC) features abundant stromal cells with an excessive extracellular matrix (ECM), termed the desmoplastic reaction. CXCR4 is a cytokine receptor for stromal cell-derived factor-1 (CXCL12) expressed in PDAC, but its roles in PDAC and the characteristic desmoplastic reaction remain unclear. Here, we generated a mouse model of PDAC with conditional knockout of Cxcr4 (KPC-Cxcr4-KO) by crossing Cxcr4 flox mice with Pdx1-Cre;KrasLSL-G12D/+;Trp53LSL-R172H/+ (KPC-Cxcr4-WT) mice to assess the development of pancreatic intraepithelial neoplasia (PanIN) and pancreatic cancers. Tumor cell characteristics of those two types were analyzed *in vitro*. In addition, CXCR4 expression in human pancreatic cancer specimens was evaluated by IHC staining. In KPC-Cxcr4-KO mice, the number and pathologic grade of PanIN lesions were reduced, but the frequency of pancreatic cancers did not differ from that in KPC-Cxcr4-WT mice. The pancreatic tumor phenotype in KPC-Cxcr4-KO mice was significantly larger and undifferentiated, characterized by abundant vimentin-expressing cancer cells, significantly fewer fibroblasts, and markedly less deposition of ECM. *In vitro*, KPC-Cxcr4-KO tumor cells exhibited higher proliferative and migratory activity than KPC-Cxcr4-WT tumor cells. Myofibroblasts induced invasion activity in KPC-Cxcr4-WT tumor cells, showing an epithelial–mesenchymal interaction, whereas KPC-Cxcr4-KO tumor cells were unaffected by myofibroblasts, suggesting their unique nature. In human pancreatic cancer, undifferentiated carcinoma did not express CXCR4 and exhibited histologic and IHC features similar to those in KPC-Cxcr4-KO mice. In summary, the CXCL12/CXCR4 axis may play an important role in the desmoplastic reaction in PDAC, and loss of CXCR4 induces phenotype changes in undifferentiated carcinoma without a desmoplastic reaction.

Significance: The current study uncovers CXCR4 as a key regulator of desmoplastic reaction in PDAC and opens the way for new therapeutic approaches to overcome the chemoresistance in patients with PDAC.

Introduction

Pancreatic ductal adenocarcinoma (PDAC) is a highly lethal disease. Despite progression in the development of therapies, the 5-year survival rate of PDAC remains around 5% to 10% because of its resistance to anticancer drugs (1, 2). Therefore, novel therapeutic targets of PDAC are urgently needed and clarifying the molecular mechanisms of this distinct disease can critically contribute to patient management.

Pancreatic lesions are considered to progress step-by-step due to multiple genetic alterations. PDAC arises from precancerous lesions with a ductal morphology, termed pancreatic intraepithelial neoplasia (PanIN; ref. 3). On the basis of findings from a pancreatic cancer mouse model, pancreatic cells bearing mutant *Kras* transform into PanIN through acinar-to-ductal metaplasia, which eventually progresses to PDAC. Several genetic alterations, transcriptional factors, and chemokines are involved in the transformation (3, 4).

A characteristic pathologic feature of PDAC is the abundance of stromal tissues, including activated fibroblasts (myofibroblasts) and extracellular matrix (ECM), referred to as the desmoplastic reaction (5), which is considered to be a major contributor to chemoresistance in PDAC. Although a number of previous works have identified pathways and fibroblast subtypes involved in the deposition of matrix in PDAC, the mechanism leading to the desmoplastic response has not been fully elucidated yet (6–8). On the other hand, a pancreatic cancer with few fibroblasts also exists. Undifferentiated carcinoma of the pancreas is a rare malignant epithelial neoplasm accounting for 0.8% to 5.7% of pancreatic cancer (9) that exhibits more aggressive clinical behavior and has a poorer prognosis than conventional PDAC (10). Its pathologic features include the lack of cell differentiation, such as keratinization, glandular structure, or mucin production, and also fewer desmoplastic changes. The reasons for these differences between conventional PDAC and undifferentiated carcinoma of the pancreas, however, are not well understood.

Stromal cell–derived factor-1, now termed CXCL12, is a homeostatic chemokine that signals through its receptor CXCR4. CXCL12 and CXCR4 have a wide range of important roles in development, including hematopoiesis and immune system organization (11). CXCR4 is a G-protein–coupled receptor encoded on chromosome

[1]Department of Gastroenterology and Hepatology, Kyoto University Graduate School of Medicine, Sakyo-ku, Kyoto, Japan. [2]Department of Gastroenterology, Kobe University Graduate School of Medicine, Kobe, Hyogo, Japan. [3]Laboratory of Stem Cell Biology and Developmental Immunology, Graduate School of Frontier Biosciences and Graduate School of Medicine, Osaka University, Osaka, Japan. [4]Kansai Electric Power Hospital, Fukushima-ku, Osaka, Japan.

Note: Supplementary data for this article are available at Cancer Research Online (http://cancerres.aacrjournals.org/).

Corresponding Author: Yuzo Kodama, Kobe University Graduate School of Medicine, 7-5-1 Kusunoki-cho, Chuo-ku, Kobe, Hyogo 650-0017, Japan. Phone: 817-8382-6305; Fax: 817-8382-6309; E-mail: kodama@med.kobe-u.ac.jp

Cancer Res 2020;80:4058–70

doi: 10.1158/0008-5472.CAN-19-2745

Published OnlineFirst June 30, 2020; DOI: 10.1158/0008-5472.CAN-19-2745

2 (12) that promotes the downstream protein kinase B/mitogen-activated protein kinases signaling pathway, leading to alterations in gene expression, actin polymerization, cell skeleton rearrangement, and cell migration (12). CXCR4 is expressed in many types of cancer cells, including PDAC, and is involved in growth, invasion, metastasis, and prognosis (13–17). Stimulation of CXCL12, which is mainly secreted by fibroblasts, increases the proliferation activity of cancer cells *in vivo* (18). Evaluation of tumors using *Cxcr4* global knockout (KO) or conditional-KO mice, however, has not been reported.

In the current study, we investigated how CXCR4 in epithelial cells affects the initiation and characteristics of PDAC using a mouse model with pancreas-specific *Cxcr4* deletion. Here, we provide evidence that CXCR4 plays a pivotal role in the desmoplastic changes in PDAC through cross-talk with CXCL12 from myofibroblasts.

Materials and Methods

Human samples

For IHC and hematoxylin and eosin (H&E) staining of human samples, surgically resected specimens were obtained from patients with PDAC or pancreatic undifferentiated carcinoma who had been admitted to Kyoto University Hospital (Kyoto, Japan).

Animals

All procedures were performed when mice were anesthetized by isoflurane (Pfizer) and all efforts were made to minimize the number of animals used and their suffering. *Cxcr4 flox* mice (19), *Pdx1-Cre* mice (20), *LSL-Kras*$^{G12D/+}$ mice (21), and *LSL-Trp53*$^{R172H/+}$ mice (22) were described previously. All mice were maintained on a mixed background.

Cell culture

All tumor tissues were isolated by surgical dissection from *KPC-Cxcr4* wild-type (WT) mice and *KPC-Cxcr4-KO* mice in 2017. Three primary culture cell lines were established from each of the tumors arising from the two strains of mice (no authentication). The fibroblasts we used were established from pancreatic tissues of C57BL/6 mice by conventional primary culture method without immortalization (no authentication). Homologous recombination in *Cxcr4*$^{flox/flox}$, *Kras*$^{LSL\text{-}G12D/+}$, or *Trp53*$^{LSL\text{-}R172H/+}$ was confirmed by PCR using primers in Supplementary Table S1. Cells were maintained at 37°C under a humidified atmosphere of 5% CO_2 in DMEM) (Gibco) growth medium supplemented with 10% FBS (Gibco) and 100 μg/mL each of penicillin and streptomycin (Invitrogen). Cell passage were conducted every 24 to 48 hours before confluence. Five to 10 passage cells were used for experiments. *Mycoplasma* testing was conducted and confirmed negative using MycoAlert (Lonza) on February 5, 2020.

Cell culture using two chamber wells (Transwell clear insert 6 wells; Corning) was performed to assess the activation of myofibroblasts by tumor cells. Myofibroblasts (3×10^5 cell/wells) derived from C57BL/6 mice pancreatic stellate cells were seeded in lower wells and incubated overnight in DMEM/10% FBS. After incubation, the medium was changed to serum-free DMEM incubated for starvation, and incubated for 24 hours. *KPC-Cxcr4-WT* and *KPC-Cxcr4-KO* tumor cells (3×10^5 cells/well) were seeded on upper chambers of other wells (pore size 0.4 μm) and incubated overnight in DMEM/10%FBS. After washing with PBS, upper chambers with tumor cells from each strain were placed on the lower wells with myofibroblasts and incubated for 24 hours. Then, the concentration of collagen 1a1 in each culture medium were measured by ELISA.

Histology

Tissues were sliced at 5 to 10 μm, fixed in 10% neutral phosphate-buffered formalin, embedded in paraffin, and stained with H&E.

IHC

The IHC study was performed according to the standard method. For mouse Cxcr4 staining, tissue sections were dephosphorylated by Lambda Phosphatase treatment (Santa Cruz Biotechnology) for 30 minutes at room temperature followed by antigen retrieval with autoclave treatment (10 mmol/L citrate buffer, ph6). For human Cxcr4 staining, antigen retrieval was performed by autoclave (ph9 tris-EDTA buffer) without dephosphorylation. Primary antibodies used in this study are listed in Supplementary Table S2. Sections were incubated overnight with primary antibodies at 4°C. The peroxidase reaction was carried out with Liquid DAB+ Substrate Chromogen System (Dako). Finally, slides were counterstained with hematoxylin (Wako).

Alcian blue staining

Alcian blue staining was performed as described previously (23). Briefly, slides were stained with pH 2.5 Alcian blue solution for 45 minutes at room temperature and counterstained with nuclear fast red solution (Sigma-Aldrich) for 10 minutes.

Sirius red staining

Sirius red staining was performed according to a general manual. Briefly, slides were stained in Picro-sirius red solution for 45 minutes at room temperature, then rinsed twice quickly with acetic acid solution followed by ethanol.

Quantitative RT-PCR

Total RNA was extracted from the pancreatic tissues or cell lines collected in RNA Later (Thermo Fisher Scientific) using an RNeasy Kit (QIAGEN) according to the manufacturer's instructions. For complementary DNA synthesis, 1 μg of total RNA was reverse-transcribed using ReverTra Ace qPCR RT Master Mix (Toyobo) and subjected to quantitative RT-PCR. Quantitative RT-PCR was performed by using the LightCycler system (Roche). The mRNA expression of specific genes was measured using FastStart Universal SYBR Green Master (Roche). RNA levels were normalized to the level of the housekeeping gene, *GAPDH*, and calculated as the Δ–Δ threshold cycle (ΔC_t). Primers used for quantitative RT-PCR are listed in Supplementary Table S1. All reactions were performed in triplicate

ELISA

Collagen 1a1 in the culture medium was quantified using Simple-Step ELISA KIT (Abcam: ab 229425) according to the manufacturer's instructions. Briefly, 100 μL of 20-fold diluted culture solution was incubated on an ELISA Kit plate coated with mouse pro-collagen 1a1 for 1 hour at room temperature and shaken at 400 rpm. After three washes with washing solution and subsequent removal of the solution, 100 μL of the reaction substrate was added to each well and the plate was incubated for 10 minutes in the dark on a plate shaker set to 400 rpm. After adding 100 μL of stopping solution, absorbance was determined at OD 450 nm. Control wells that were not coated with candidate proteins were also used as a negative control for each of the serum studies. All assays were performed in triplicate.

Proliferation assay

KPC-Cxcr4-WT and *KPC-Cxcr4-KO* tumor cells (2×10^3 cells/well) were seeded in 96-well plates and cultured in DMEM/10% FBS. The medium was changed to serum-free DMEM for overnight incubation.

Published OnlineFirst June 30, 2020; DOI: 10.1158/0008-5472.CAN-19-2745

Cell growth was analyzed at 24 and 48 hours using the MTS Reagent Kit (Promega) added 1 hour before taking the spectrophotometric reading, according to the manufacturer's directions.

In vitro wound-healing assays

Wound-healing assays were evaluated with *KPC-Cxcr4-WT* and *KPC-Cxcr4-KO* tumor cells. Cells (1×10^4 cells/well) were seeded in 12-well plates and grown into a monolayer. A pipette was used to scratch the monolayer and the medium was replaced with serum-free medium. After 20 hours, the wound closure percentage in 8 high-power fields (HPF) were quantified by ImageJ software analysis.

Experimental model of liver metastases

Ten-week-old C57BL/6 mice were anesthetized with isoflurane. Tumor cells (2×10^5) derived from *KPC-Cxcr4-WT* and *KPC-Cxcr4-KO* mice were suspended in DMEM/10% FBS. The cells were injected in the mouse spleens with a 27G syringe during open laparotomy. After 3 weeks, the number of liver metastases at the liver surface was counted.

Microarray analysis

Total RNA from each of the 3 *KPC-Cxcr4-WT* and *KPC-Cxcr4-KO* tumor cell cultures was examined using the SurePrint G3 Mouse Gene Expression 8 × 60K v2 (Agilent Technologies). Gene expression data were analyzed using gene set enrichment analysis (GSEA) software and the Molecular Signature Database (MsigDB).

Cell invasion assay

The invasion assay was performed using a Transwell invasion assay (Corning) with 24 wells according to the manufacturer's instructions. Briefly, *KPC-Cxcr4-WT* and *KPC-Cxcr4-KO* tumor cells (2×10^3 cells/well) were placed in the upper chambers of Matrigel-coated 8-μm transwells. The bottom chambers were seeded with myofibroblasts (2×10^3 cell/well) derived from C57BL/6 mice pancreatic stellate cells filled with serum-free DMEM and incubated for 48 hours. After incubation for 20 hours, noninvading cells were carefully removed with a cotton swab. Cells that had penetrated through the Matrigel located on the underside of the filter were fixed with cold methanol for 15 minutes, then stained with Crystal violet and the number of invading cells was counted. Anti-CXCL12 antibody (Abcam; ab9797) was added to some wells to confirm that the myofibroblast-induced invasion was blocked.

Statistical analysis

Statistical analysis was performed using JMP (SAS Institute) or Excel (Microsoft Corp.) software. Intergroup comparisons were performed using Student *t* test for normally distributed unpaired data and the Mann–Whitney U test for nonnormally distributed unpaired data. Differences were assessed using Student *t* test, log-rank test, ANOVA test, and Fisher exact test for categorical data. A *P* value of <0.05 was considered statistically significant. For *P* values, the following scale was applied: *, $P < 0.05$; **, $P < 0.01$; and ***, $P < 0.001$. Data are presented as means ± SEM. Five to 10 nonoverlapping HPFs were analyzed by counting positive cells or measuring positive area for each staining. Each area was evaluated by ImageJ software.

In **Fig. 6Q**, it was judged as positive when Cxcr4 was more than 70% positive in those cancer cells.

Study approval

All animal care and experiments were conducted according to the guidelines for the Japan's Act on Welfare and Management of Animals. All animal experiments and materials and methods described herein were approved by the review board of Kyoto University Graduate School (Kyoto, Japan). Written informed consent for the use of their resected tissues were obtained from all patients in accordance with the Declaration of Helsinki.

Results

PanIN formation was reduced in Cxcr4 conditional KO mice

To investigate the role of Cxcr4 in pancreatic development, we first evaluated the phenotype of pancreas-specific KO of the *Cxcr4* gene by analyzing *Pdx1-Cre;Cxcr4*$^{flox/flox}$ (*Cxcr4-KO*) mice (Supplementary Fig. S1A). Successful *Cxcr4* gene recombination in pancreatic tissue was confirmed by PCR (Supplementary Fig. S1B and S1C). We observed *Cxcr4-KO* mice for up to 48 weeks of age, but detected no abnormalities or body weight loss compared with *Pdx1-Cre;Cxcr4*$^{WT/WT}$ (*Cxcr4-WT*) mice (Supplementary Fig. S1D). Histologic analysis by H&E staining and IHC for amylase and insulin also showed no abnormalities in pancreatic exocrine and endocrine tissues in the *Cxcr4-KO* mice (Supplementary Fig. S1E–S1L), suggesting that *Cxcr4* KO does not affect pancreatic development.

Next, to evaluate the role of Cxcr4 in the development of PanIN and PDAC, we crossed *Cxcr4*$^{flox/flox}$ mice with *Pdx1-Cre;Kras*$^{LSL\text{-}G12D/+}$;*Trp53*$^{LSL\text{-}R172H/+}$ (*KPC-Cxcr4-WT*) mice and generated *Pdx1-Cre;Kras*$^{LSL\text{-}G12D/+}$;*Trp53*$^{LSL\text{-}R172H/+}$;*Cxcr4*$^{flox/flox}$ *(KPC-Cxcr4-KO)* mice (**Fig. 1A**). The KPC mouse model is reported to develop PanIN and PDAC within 4 and 16 to 20 weeks, respectively (24), and therefore, we evaluated PanIN lesion formation in *KPC-Cxcr4-WT* and *KPC-Cxcr4-KO* mice by H&E staining and Alcian blue staining at 16 weeks of age. PanIN developed in both mouse strains, but the area of PanIN analyzed by Alcian blue staining was significantly smaller in *KPC-Cxcr4-KO* mice than in *KPC-Cxcr4-WT* mice (11.3% vs. 23.5%, $P = 0.02$; **Fig. 1B–E** and **H**). IHC revealed weaker expression of phosphorylated ERK (pERK), a downstream of Cxcr4, in PanIN lesions of *KPC-Cxcr4-KO* mice than those of *KPC-Cxcr4-WT* mice (**Fig. 1F** and **G**). In addition, not only the total number of PanIN lesions, but also the grade was significantly lower in *KPC-Cxcr4-KO* mice than in *KPC-Cxcr4-WT* mice (**Fig. 1I**). These findings indicate that Cxcr4 promotes the initiation and development of PanIN.

Undifferentiated pancreatic cancer without a desmoplastic reaction formed in *Cxcr4 conditional KO mice*

We next analyzed PDAC formation in *KPC-Cxcr4-KO* mice at 16 to 20 weeks of age. Although PanIN development in *KPC-Cxcr4-KO* mice was much lower, as described above, the pancreatic tumor formation rate did not differ between *KPC-Cxcr4-KO* and *KPC-Cxcr4-WT* mice (23.0% vs. 26.3%, $P = 0.62$; **Fig. 2A**). In addition, overall survival time did not differ between *KPC-Cxcr4-KO* and *KPC-Cxcr4-WT* mice (**Fig. 2B**). The morphology of the developed tumors, however, markedly differed between the two strains of mice. Tumors that formed in *KPC-Cxcr4-KO* mice were significantly larger than those in *KPC-Cxcr4-WT* mice (12.3 mm vs. 7.4 mm, $P = 0.039$; **Fig. 2C**), and the tumor boundaries were unclear, suggesting more aggressive and invasive characteristics (**Fig. 2D** and **E**). The number of Ki67-positive cells was significantly higher in tumors of *KPC-Cxcr4-KO* mice than those of *KPC-Cxcr4-WT* mice, confirming this higher proliferative phenotype (100.5 vs. 37.5 $P = 0.049$; **Fig. 2F–H**). Regarding angiogenesis, IHC analysis showed that the area of CD31-positive cells in the tumor did not differ between *KPC-Cxcr4-KO* and *KPC-Cxcr4-WT* mice (1.96% vs. 1.97% $P = 0.98$; **Fig. 2I–K**). Histologic analysis by

Published OnlineFirst June 30, 2020; DOI: 10.1158/0008-5472.CAN-19-2745

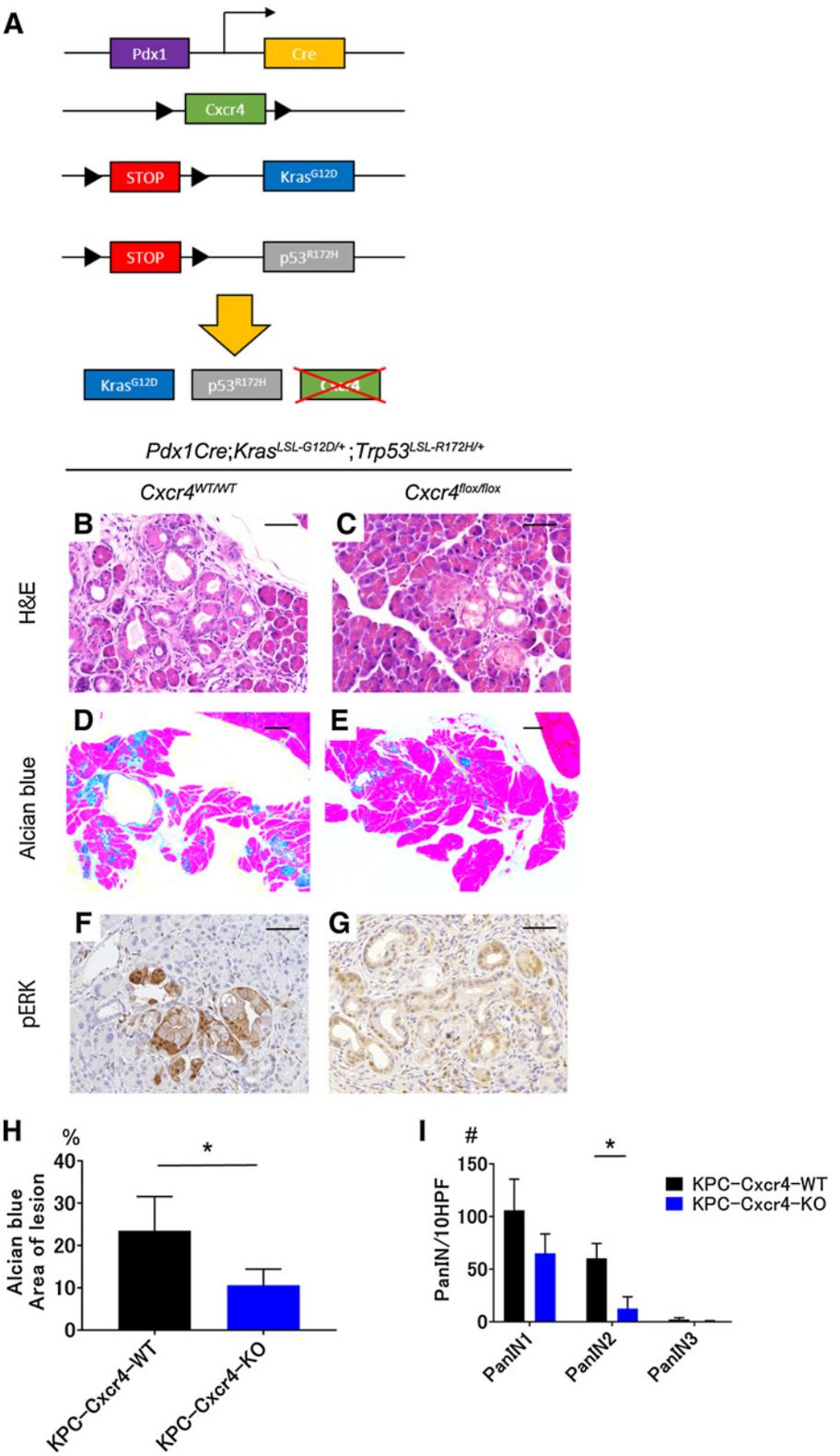

Figure 1.

PanIN formation was reduced in *Cxcr4* conditional KO mice. **A,** Design of *Cxcr4* flox mouse model used in this study, which employs the *Kras*$^{LSL\text{-}G12D/+}$, *Pdx1-Cre, Trp53*$^{LSL\text{-}R172H/+}$, and *Cxcr4* alleles. Cre-mediated deletion results in the expression of mutated *Kras* and *Trp53* genes and deletion of both alleles of *Cxcr4*. **B** and **C,** H&E staining of pancreatic lesions of *KPC-Cxcr4-WT* (**B**) and *KPC-Cxcr4-KO* (**C**) mice at 16 weeks. **D** and **E,** Alcian blue staining showing representative histology from *KPC-Cxcr4-WT* (**D**) and *KPC-Cxcr4-KO* (**E**) mice at 16 weeks. **F** and **G,** IHC for pERK of *KPC-Cxcr4-WT* (**F**) and *KPC-Cxcr4-KO* (**G**) mice at 16 weeks. **H,** Area of PanIN lesions in *KPC-Cxcr4-WT* and *KPC-Cxcr4-KO* mice ($n = 4/6$). **I,** Numbers of PanIN lesions for each grade in *KPC-Cxcr4-WT* and *KPC-Cxcr4-KO* mice ($n = 5$ for each group). PanIN grades were classified into three groups (PanIN1, PanIN2, and PanIN3). Ten nonoverlapping HPFs were analyzed. *, $P < 0.05$, Student *t* test. Scale bars, 50 μm (**B**, **C**, **F**, and **G**); 2 mm (**D** and **E**).

Published OnlineFirst June 30, 2020; DOI: 10.1158/0008-5472.CAN-19-2745

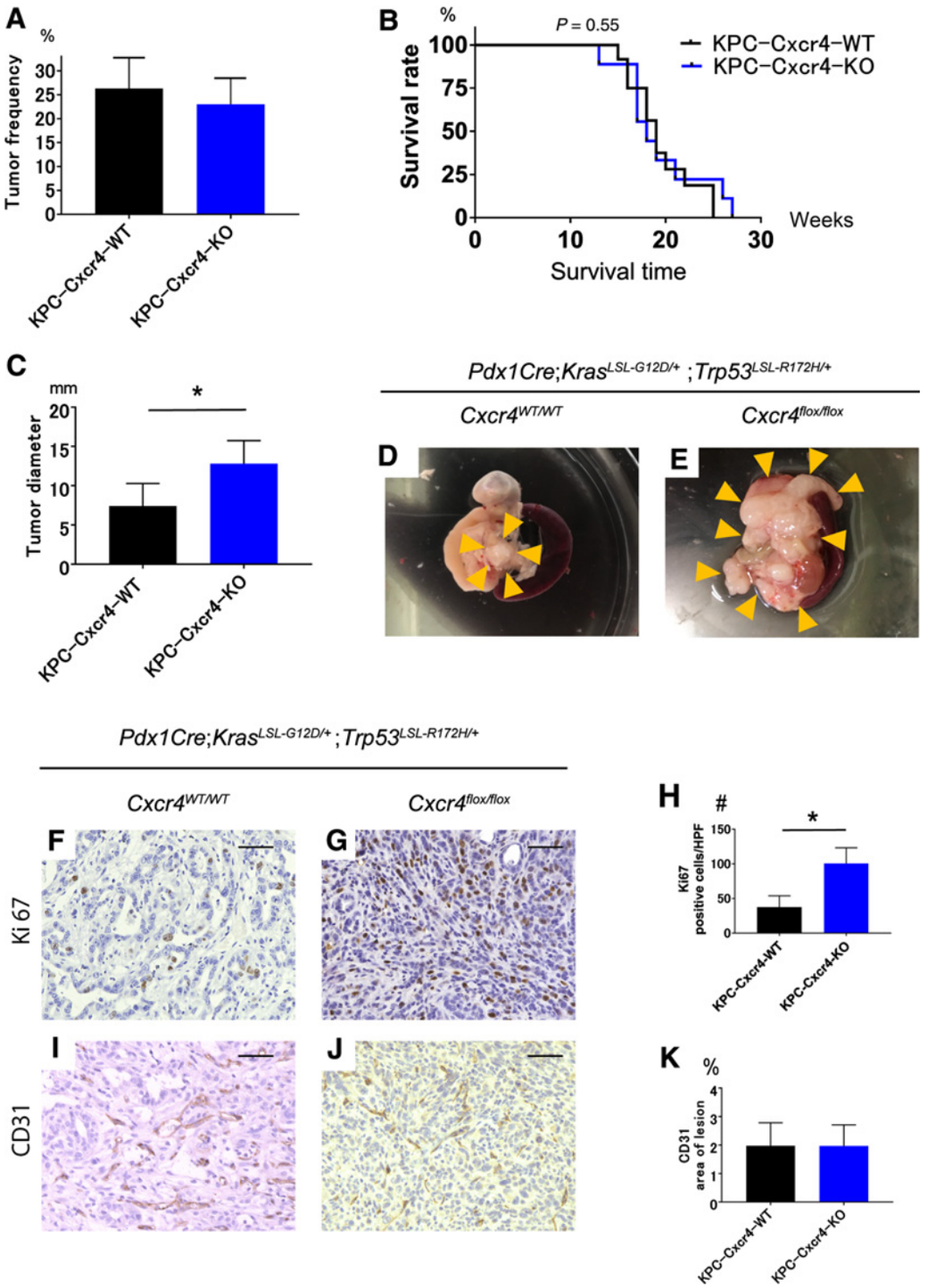

Figure 2.

Cxcr4 conditional-KO did not affect the incidence of pancreatic tumors but increased their size. **A,** Frequency of pancreatic tumors in *KPC-Cxcr4-WT* (26.3 %, 5/19) and *KPC-Cxcr4-flox* (23.0 %, 5/22) mice at 16 to 20 weeks. $P = 0.79$. Fisher exact test. **B,** Kaplan–Meier survival data showed that the survival rate of *KPC-Cxcr4-WT* and *KPC-Cxcr4-KO* mice did not differ ($n = 14/12$). $P = 0.55$, log-rank test. **C,** Average tumor diameter of *KPC-Cxcr4-WT* and *KPC-Cxcr4-KO* tumors ($n = 5/5$). **D** and **E,** Macroscopic view of pancreatic tumors from *KPC-Cxcr4-WT* (**D**) and *KPC-Cxcr4-KO* (**E**) mice. Yellow arrowheads show the border of tumor. **F** and **G,** IHC for Ki67 of *KPC-Cxcr4-WT* (**F**) and *KPC-Cxcr4-KO* (**G**) tumors. **H,** Histologic analysis of Ki67-positive tumor cells in *KPC-Cxcr4-WT* and *KPC-Cxcr4-KO* mice ($n = 3/3$). Five to 10 nonoverlapping HPFs were analyzed. **I** and **J,** IHC for CD31 of *KPC-Cxcr4-WT* (**I**) and *KPC-Cxcr4-KO* (**J**) tumors. **K,** Percentage of CD31-positive tumor cells ($n = 3/3$). Five to 10 nonoverlapping HPFs were analyzed. Values in graphs are mean ± SEM. *, $P < 0.05$ Student *t* test (**C**, **H**, and **K**). Scale bars, 50 μm.

Published OnlineFirst June 30, 2020; DOI: 10.1158/0008-5472.CAN-19-2745

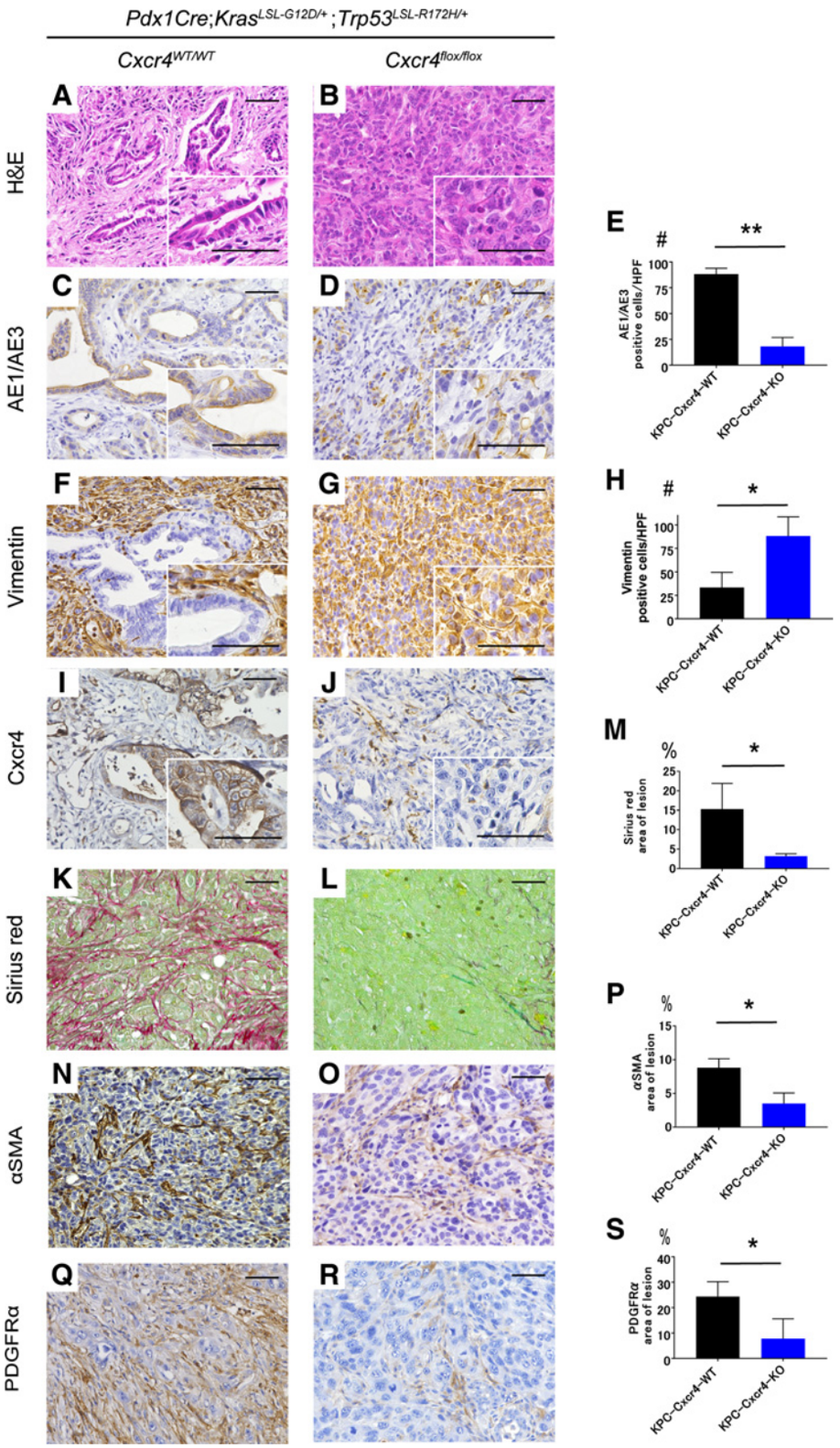

Figure 3.

Undifferentiated pancreatic cancer without a desmoplastic reaction was formed in *Cxcr4* conditional-KO mice. Histologic analysis of tumors formed in *KPC-Cxcr4-WT* and *KPC-Cxcr4-KO* mice. **A** and **B,** H&E staining. **C** and **D,** IHC for AE1/AE3. **E,** Percentage of AE1/AE3-positive tumor cells ($n = 3/3$). **F** and **G** IHC for vimentin. **H,** Percentage of vimentin-positive tumor cells ($n = 3/3$). **I** and **J,** IHC for Cxcr4. **K** and **L,** Picro-sirius red staining. **M,** Picro-sirius red-positive area ($n = 4/4$). **N** and **O,** IHC for αSMA. **P,** αSMA-positive area ($n = 4/4$). **Q** and **R,** IHC for PDGFRα. **S,** PDGFRα-positive area ($n = 3/3$). Values in graphs are mean ± SEM. *, $P < 0.05$; **, $P < 0.01$, Student *t* test. Scale bars, 50 μm. Five to 10 non-overlapping HPFs were analyzed.

Published OnlineFirst June 30, 2020; DOI: 10.1158/0008-5472.CAN-19-2745

H&E staining and IHC for pan-cytokeratin (AE1/AE3) and vimentin showed typical images of ductal adenocarcinoma with pan-cytokeratin–positive cancer cells and abundant vimentin-positive cancer-associated fibroblasts in the tumors of *KPC-Cxcr4-WT* mice (**Fig. 3A**, **C**, **F**, and **E**). In contrast, the tumors of *KPC-Cxcr4-KO* mice exhibited a higher density of cancer cells with pleomorphic nuclei that weakly expressed pan-cytokeratin and strongly expressed vimentin, but the characteristic desmoplastic changes were not observed (AE1/AE3 88.3% vs. 3.3% $P < 0.01$, vimentin 33.4% vs. 88.2% $P = 0.02$; **Fig. 3B**, **D**, **G**, and **H**). IHC for Cxcr4 revealed Cxcr4 expression in cancer cells in *KPC-Cxcr4-WT* mice and loss of its expression in *KPC-Cxcr4-KO* mice (**Fig. 3I** and **J**), whereas expressions of Cxcr4 in immune cells in the tumor microenvironment as well as in the spleen were equivalently observed in both strains of mice (Supplementary Fig. S2A and S2B). Picro-sirius red staining and IHC for α-smooth muscle actin (αSMA) and PDGFRα revealed significantly lower collagen deposition and myofibroblast activation, respectively, in tumors of *KPC-Cxcr4-KO* mice compared with *KPC-Cxcr4-WT* mice (Picro-sirius red; 15.3% vs. 3.2% $P = 0.027$, αSMA; 8.8% vs. 3.5% $P = 0.002$, PDGFRα; 24.4% vs. 3.4% $P = 0.042$; **Fig. 3K** and **S**), confirming the phenotype of a decreased desmoplastic reaction in tumors of *KPC-Cxcr4-KO* mice. We also performed IHC for CD3, CD8, Gr1, F4/80 to evaluate infiltration of immune cells. As a result, a substantial number of F4/80-positive monocytes and a few CD3-positive T cells were found in the tumors, but few CD8-positive T cells and Gr1-positive neutrophils were observed. Importantly, we could not find any differences in the infiltrations of these immune cells between the tumors of *KPC-Cxcr4-WT* and *KPC-Cxcr4-KO* mice (Supplementary Fig. S3A–S3I). Expression of pERK in cancer cells was weaker in *KPC-Cxcr4-KO* mice than in *KPC-Cxcr4-WT* mice (Supplementary Fig. S4A). These findings suggested that the characteristic desmoplastic reaction in PDAC is meditated by Cxcr4 in epithelial cells, and thus, conditional *Cxcr4* gene KO induces the formation of undifferentiated cancer with little stroma.

Cxcr4 KO induced aggressive characteristics in cancer cells through an epithelial–mesenchymal transition

To further examine the features of vimentin-positive tumors with the characteristic morphology in *KPC-Cxcr4-KO* mice, we established primary cancer cell lines from *KPC-Cxcr4-KO* and *KPC-Cxcr4-WT* mice using a previously reported method (25). Successful gene recombination of *Cxcr4*, $Kras^{LSL\text{-}G12D/+}$, and $Trp53^{LSL\text{-}R172H/+}$ in these cells were confirmed by PCR (**Fig. 4A**), and loss of *Cxcr4* expression was confirmed by quantitative RT-PCR analysis and immunofluorescent analysis (**Fig. 4B** and **C**). Quantitative RT-PCR analysis also showed a complete loss of *Epcam* mRNA expression and a marked increase in *vimentin* mRNA expression in cancer cells derived from *KPC-Cxcr4-KO* mice compared with *KPC-Cxcr4-WT* mice (**Fig. 4D** and **E**), confirming the results of the IHC for pan-cytokeratin and vimentin. Under these conditions, an MTS assay (**Fig. 4F**) and wound-healing assay (**Fig. 4G** and **H**) revealed that cancer cells from *KPC-Cxcr4-KO* mice exhibited significantly higher proliferative activity and migratory activity (78% vs. 39%, $P = 0.03$; wound-healing assay could be affected by proliferative activity), respectively, than cancer cells from *KPC-Cxcr4-WT* mice. Microarray analysis using these tumor cells revealed reduced Kras/MAPK signaling, decreased Syk expression that promotes epithelial differentiation, and increased epithelial mesenchymal transition (EMT)–related gene expression in cancer cells from *KPC-Cxcr4-KO* mice (Supplementary Fig. S4B). Furthermore, GSEA on RNA sequence data showed upregulation of EMT-related gene expression in cancer cells from *KPC-Cxcr4-KO* mice (Supplementary Fig. S4C). Both cell lines from *KPC-Cxcr4-KO* and *KPC-Cxcr4-WT* mice did not express Cola1a1 mRNA, suggesting no stromal contamination (Supplementary Fig. S5A).

Thus, in contrast to previous reports using CXCR4 inhibitors or knockdown (26, 27), *CXCR4* KO induced an EMT and stimulated the proliferation and migration of tumor cells both *in vivo* and *in vitro*.

On the other hand, CXCR4 is known to play a definitive role in promoting cancer metastasis. Because *KPC-Cxcr4-KO* and *KPC-Cxcr4-WT* mice did not have spontaneous metastasis during their lifetime, we next analyzed the metastatic ability of cancer cells by splenic injection. Consistent with previous reports (17), the number of liver metastases was significantly lower in cancer cells from *KPC-Cxcr4-KO* mice than in those from *KPC-Cxcr4-WT* mice (Supplementary Fig. S6A–S6F), suggesting that the CXCL12/CXCR4 axis is important for metastasis.

Myofibroblasts induced cancer cell migration through the CXCL12/CXCR4 axis

To elucidate the characteristic tumor phenotype without a desmoplastic reaction of *KPC-Cxcr4-KO* tumor cells, we focused on epithelial–mesenchymal interactions between cancer cells and myofibroblasts. We first assessed the effects of secretory factors from cancer cells on myofibroblasts utilizing a two chamber assay in which cancer cells from *KPC-Cxcr4-KO* or *KPC-Cxcr4-WT* mice were placed into the upper chamber and myofibroblasts were seeded into the lower chamber and cultured for 24 hours (**Fig. 5A**). On the basis of the concentration of collagen 1a1 in the culture media, cancer cells from both strains activated myofibroblasts compared with myofibroblasts without tumor cells, but there were no differences between strains (**Fig. 5B**). mRNA expression of *αSMA* in myofibroblasts also did not differ between strains. (**Fig. 5C**). Next, we evaluated the effects of myofibroblasts on cancer cells using the two-chamber invasion assay. After culturing myofibroblasts for 24 hours in the lower wells, cancer cells from *KPC-Cxcr4-KO* or *KPC-Cxcr4-WT* mice were placed in the upper wells and their invasion ability was evaluated after 20 hours (**Fig. 5D**). Myofibroblasts strongly induced cell migration across the well of cancer cells from *KPC-Cxcr4-WT* mice, but not of cancer cells from *KPC-Cxcr4-KO* mice (**Fig. 5E**), while both types of tumors migrated little without myofibroblasts during the observation time. Furthermore, this migratory effect of cancer cells from *KPC-Cxcr4-WT* mice was markedly inhibited by treatment with the anti-CXCL12 antibody (**Fig. 5F**). Together with our findings that Cxcl12 is produced by myofibroblasts and not by cancer cells (Supplementary Fig. S6G), these results indicate that CXCL12 secreted from myofibroblasts induces cancer cell migration via CXCR4. Thus, cancer cells from *KPC-Cxcr4-WT* mice are likely to form a tumor microenvironment by epithelial–mesenchymal interactions through CXCL12/CXCR4 signaling, but cancer cells from *KPC-Cxcr4-KO* mice appear to survive more independently from mesenchymal cells.

Loss of CXCR4 expression was observed in human undifferentiated pancreatic cancer

We next investigated the characteristics of human undifferentiated carcinoma focusing on CXCR4. We histologically evaluated specimens of seven consecutive cases with undifferentiated pancreatic cancer surgically resected at Kyoto University Hospital from 1996 to 2014 in comparison with typical PDAC (Supplementary Table S3). In undifferentiated cancer specimens, H&E staining showed a higher density of cancer cells with pleomorphic nuclei and no desmoplastic reaction,

Published OnlineFirst June 30, 2020; DOI: 10.1158/0008-5472.CAN-19-2745

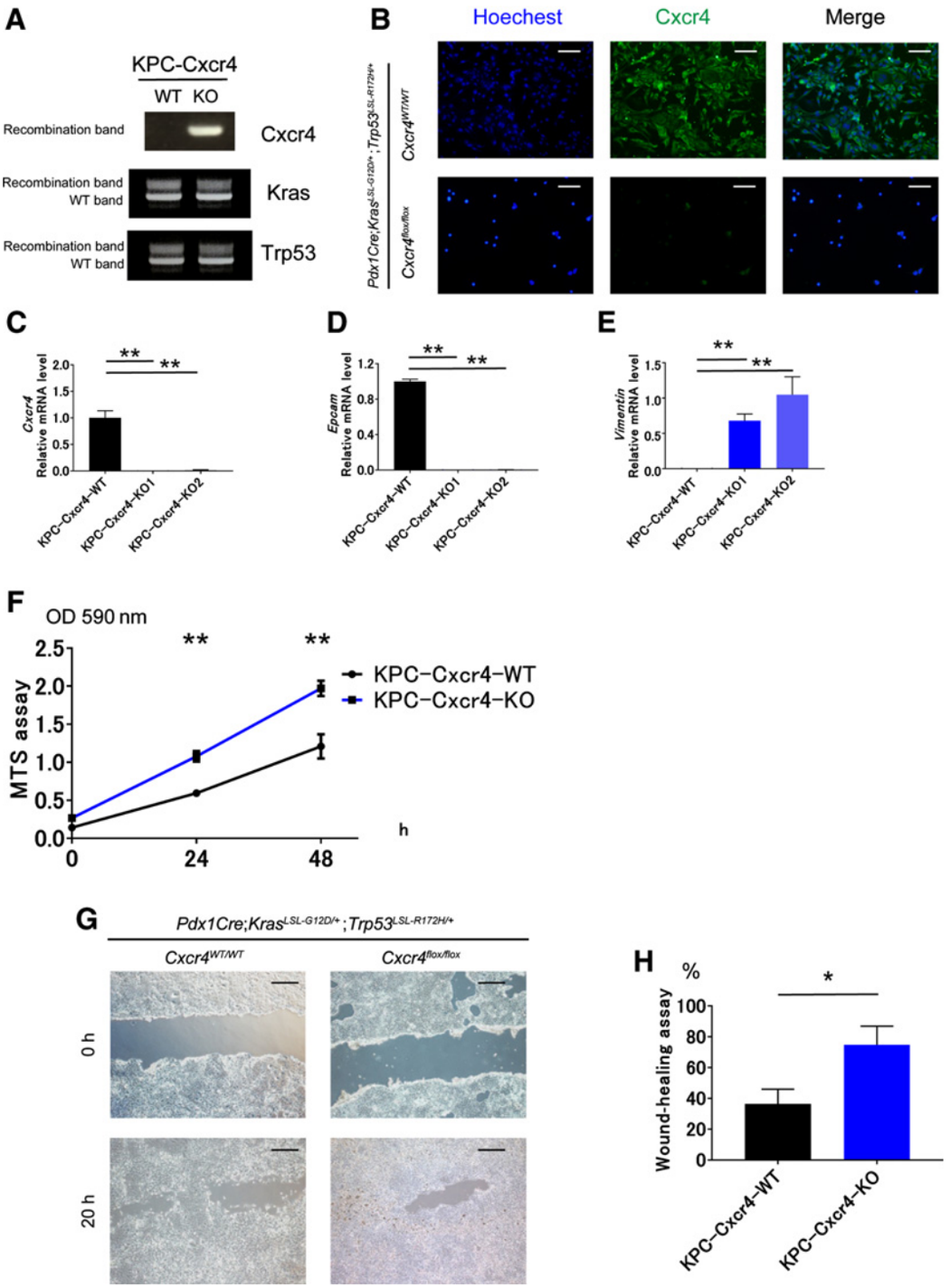

Figure 4.

Cxcr4 KO induced aggressive characteristics in cancer cells through an EMT. **A,** PCR analysis for *Cxcr4, Kras*, and *Trp53* recombination in *KPC-Cxcr4-WT and KPC-Cxcr4-KO* primary tumor cells. **B,** IHC for Cxcr4 with primary cultured tumor cells established from *KPC-Cxcr4-WT* and *KPC-Cxcr4-KO* (Hoechst, blue; Cxcr4, green). **C,** Quantitative RT-PCR analysis of *Cxcr4* mRNA expression in pancreatic tumor cells of *KPC-Cxcr4-WT* and *KPC-Cxcr4-KO* tumors ($n = 3/3/3$). **, $P < 0.01$, ANOVA test. **D** and **E,** Quantitative RT-PCR analysis of *Epcam* mRNA (**D**) and *vimentin* mRNA (**E**) expressed by *KPC-Cxcr4-WT* and *KPC-Cxcr4-KO* tumor cells ($n = 3/3/3$). **, $P < 0.01$, Student *t* test. **F,** Assessment of the cell proliferation ability of *KPC-Cxcr4-WT* and *KPC-Cxcr4-KO* tumor cells using MTS assay. Each of 6 wells was analyzed. Values in graphs represent the mean ± SEM. **, $P < 0.01$, Student *t* test. **G** and **H,** Assessment of cell migration in wound closure assay was performed in *KPC-Cxcr4-WT* and *KPC-Cxcr4-KO* tumor cells at 0 and 20 hours (**G**). Quantification of wound closure after 20 hours (**H**). Values in graphs represent the mean ± SEM. *, $P < 0.05$, Student *t* test ($n = 8/8$). Scale bars, 50 μm.

Published OnlineFirst June 30, 2020; DOI: 10.1158/0008-5472.CAN-19-2745

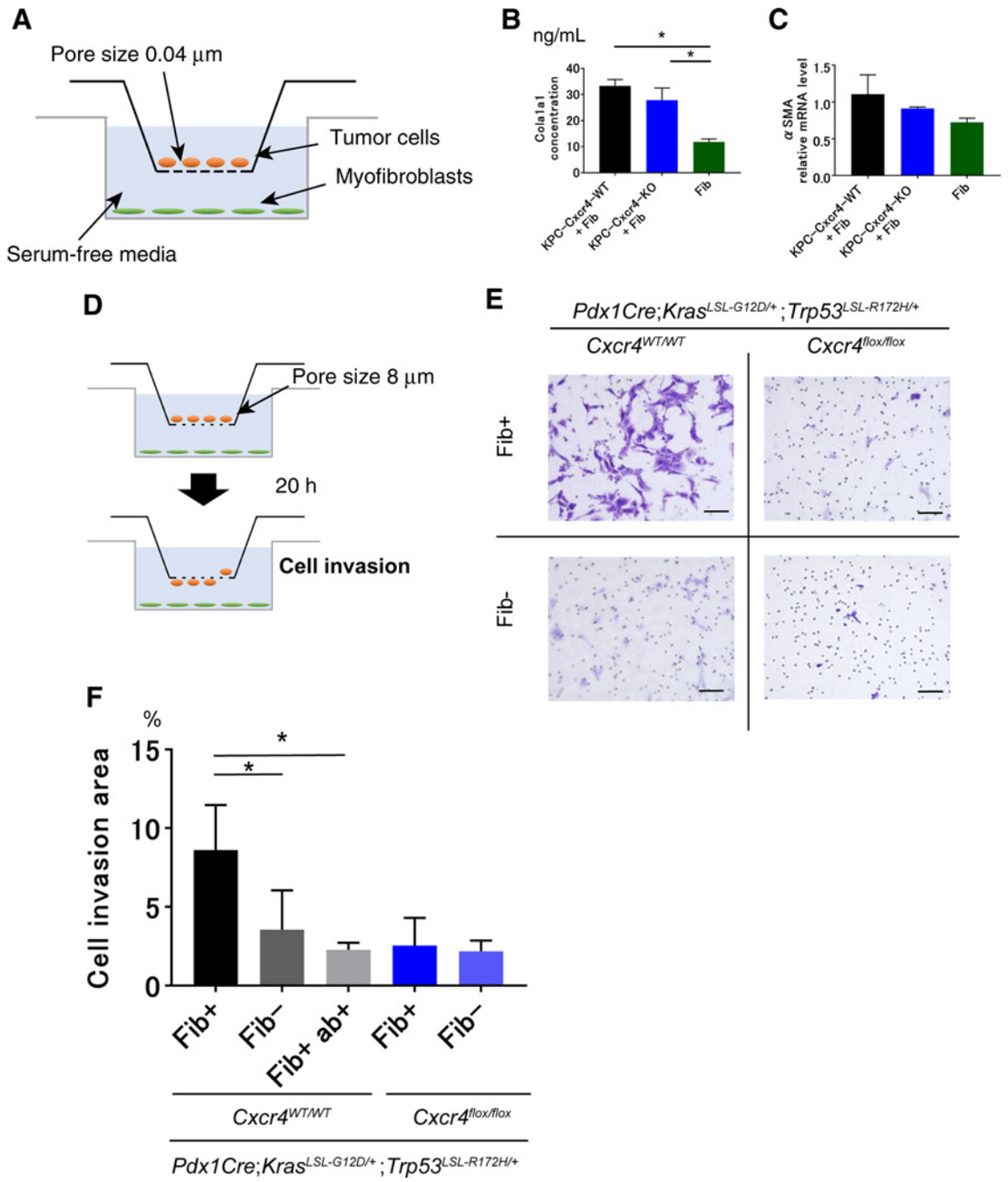

Figure 5.

Myofibroblasts induced cancer cell migration through CXCL12/CXCR4 axis. **A,** The schema of the two-chamber cell culture assay. Pore size of the upper chamber is 0.04 μm (cells cannot migrate). Tumor cells and myofibroblasts were incubated with serum-free DMEM medium. **B,** Collagen 1a1 (Cola1a1) concentration of supernatant in which *KPC-Cxcr4-WT* or *KPC-Cxcr4-KO* tumor cells or myofibroblasts (Fib) on the upper wells and myofibroblasts on the lower wells ($n = 4$ for each group) were cultured. Values in graphs are mean ± SEM. ANOVA test. **C,** Quantitative RT-PCR analysis of *αSMA* mRNA of lower well myofibroblasts in which *KPC-Cxcr4-WT* or *KPC-Cxcr4-KO* tumor cells or myofibroblasts on the upper wells ($n = 3$ for each group) were cultured. Values in graphs are mean ± SEM. ANOVA test. **D,** The schema of the two-chamber invasion assay. Pore size of the upper chamber was 8 μm (cells can migrate). Tumor cells and myofibroblasts were incubated with serum-free DMEM medium. After 20 hours, the area of invaded tumor cells was evaluated. **E,** Invasion assay was performed on *KPC-Cxcr4-WT* or *KPC-Cxcr4-KO* tumor cells with or without myofibroblasts (Fib + or Fib −) on lower wells. Invasive tumor cells were stained with Crystal violet and the numbers were counted under an inverted microscope. Scale bars, 50 μm. **F,** The areas of invading cells were analyzed statistically. *KPC-Cxcr-WT* with myofibroblasts (Fib +), $n = 6$; *KPC-Cxcr4-WT* without myofibroblasts (Fib −), $n = 3$; *KPC-Cxcr4-WT* with myofibroblasts and anti-CXCL12 antibody, $n = 3$; *KPC-Cxcr4-KO* with fibroblasts, $n = 3$; *KPC-Cxcr4-KO* without myofibroblasts, $n = 3$. The cell invasive effects of the myofibroblasts were blocked in the well to which anti-CXCL12 antibody was added. Values in graphs are mean ± SEM. *, $P < 0.05$, ANOVA test.

Published OnlineFirst June 30, 2020; DOI: 10.1158/0008-5472.CAN-19-2745

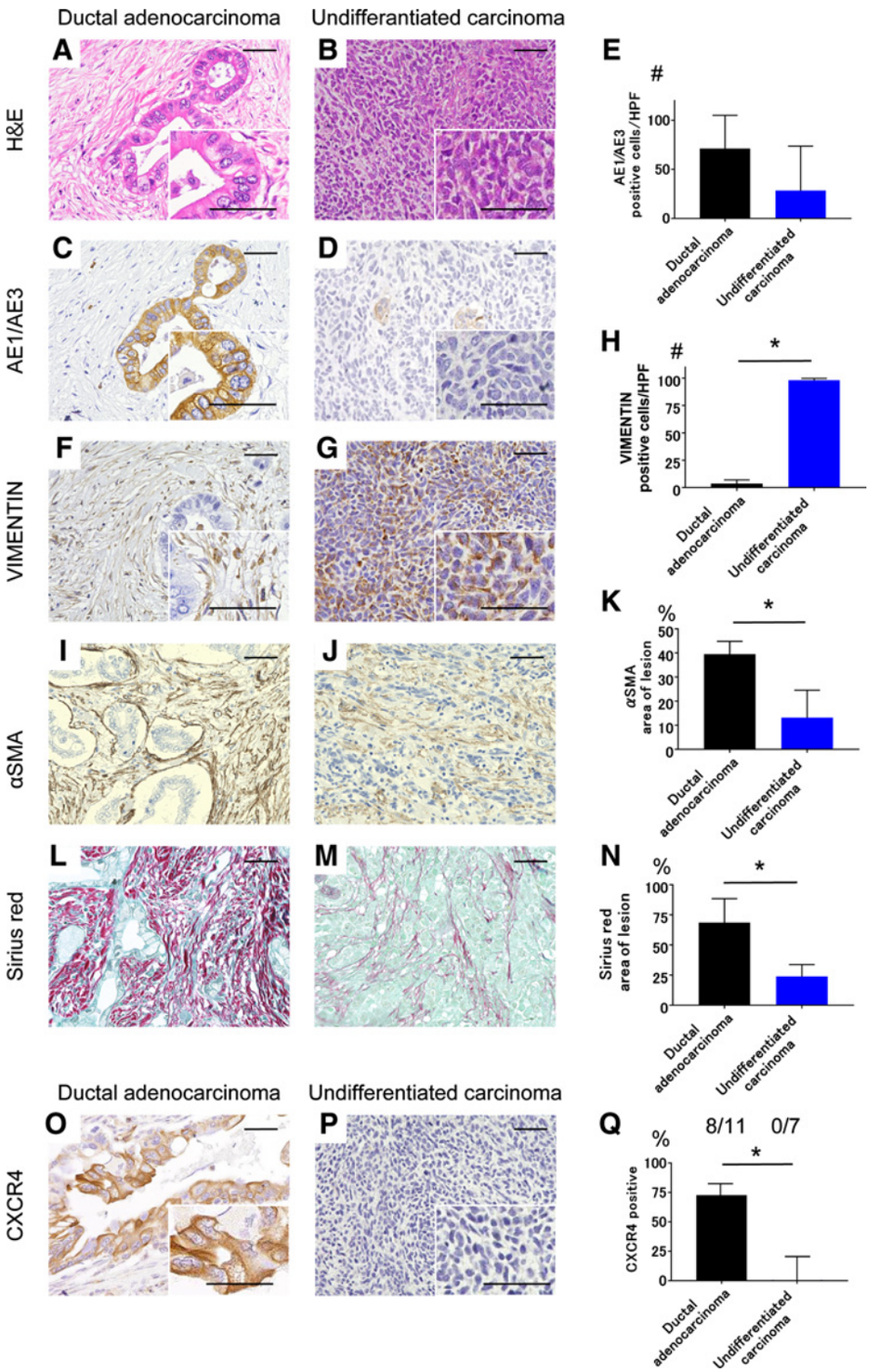

Figure 6.

Loss of CXCR4 expression was observed in human undifferentiated pancreatic cancer. **A** and **B,** PDAC (**A**) and undifferentiated carcinoma (**B**) were stained for H&E. **C** and **D,** IHC for AE1/AE3 of PDAC (**C**) and undifferentiated carcinoma (**D**). **E,** Percentage of AE1/AE3-positive tumor cells in PDAC and undifferentiated carcinoma ($n = 3/3$). **F** and **G,** IHC for vimentin of PDAC (**F**) and undifferentiated carcinoma (**G**). **H,** Percentage of vimentin-positive tumor cells in PDAC and undifferentiated carcinoma ($n = 3/3$). **I** and **J,** IHC for αSMA of PDAC (**I**) and undifferentiated carcinoma (**J**). **K,** αSMA-positive area in PDAC and undifferentiated carcinoma ($n = 3/3$). **L** and **M,** Picro-sirius red staining of PDAC (**L**) and undifferentiated carcinoma (**M**) mice. **N,** Picro-sirius red-positive area in PDAC and undifferentiated carcinoma ($n = 3/3$). **O–Q,** Immunostaining of CXCR4 protein in cancer lesion, ductal adenocarcinoma (**O**), and undifferentiated carcinoma (**P**). The rate of CXCR4-positive cancer tissues in ductal carcinoma (72.7%, 8/11) and undifferentiated carcinoma (0%, 0/7; **Q**). Values in graphs are mean ± SEM. *, $P < 0.05$, Student *t* test (**E**, **H**, **K**, and **N**) and Fisher exact test (**Q**). Scale bar, 50 μm. Five to 10 nonoverlapping HPFs were analyzed.

and IHC showed weaker pan-cytokeratin expression and stronger vimentin expression (AE1/AE3 71.4% vs. 28.4% $P = 0.26$, vimentin 3.7% vs. 98.1% $P < 0.01$; **Fig. 6A–H**). IHC for αSMA and Picro-sirius red staining revealed significantly lower fibroblast activation and collagen deposition, respectively, than in ductal adenocarcinoma (αSMA 39.5% vs. 13.1%, $P = 0.02$, Picro-sirius red 68.5% vs. 23.8% $P = 0.03$; **Fig. 6I–N**). Notably, these features of human undifferentiated pancreatic cancer were quite similar to those of the tumors that formed in *KPC-Cxcr4-KO* mice. As for CXCR4, IHC showed CXCR4 expression in 72.7% (8/11) of cases with ductal adenocarcinoma, as reported previously (Supplementary Fig. S7A–S7J; ref. 14). In contrast, CXCR4 expression was not detected in any of the cases with

Published OnlineFirst June 30, 2020; DOI: 10.1158/0008-5472.CAN-19-2745

undifferentiated cancer (0/7, 0%, $P = 0.04$; **Fig. 6O–Q**). These findings indicated that loss of CXCR4 could be associated with the development of human undifferentiated pancreatic cancer.

Discussion

PDAC is a highly lethal disease. Highly characteristic pathologic findings of PDAC are the abundant activated fibroblasts and extracellular matrix, referred to as the desmoplastic reaction. The molecular mechanisms of the desmoplastic reaction are poorly understood. In the current study, our analysis of pancreas-specific *Cxcr4* conditional-KO in a PDAC mouse model revealed that the Cxcl12/Cxcr4 axis contributes to the desmoplastic reaction. This finding was further supported by our observation that CXCR4 expression was markedly reduced in human undifferentiated pancreatic carcinoma, in which few desmoplastic reactions are seen.

First, we evaluated the role of CXCR4 in pancreatic organogenesis and maintenance of homeostasis. In general, CXCR4 is expressed on progenitor cells during embryonic development and plays a critical role in the development and differentiation of many organs (28, 29). As for the pancreas, CXCR4 is reported to be expressed on endocrine progenitor cells and to promote the proliferation and maturation of β cells (30). In contrast to previous reports, however, we found no pancreatic phenotype or growth defects in *Pdx1Cre;Cxcr4*$^{flox/flox}$ mice, in which *Cxcr4* was knocked out in both the pancreatic exocrine and endocrine tissues. Our findings suggested that CXCR4 is not essential for the development of pancreas.

Next, we analyzed the role of CXCR4 in PanIN formation. Thomas and colleagues evaluated CXCR4 expression in PanIN lesions in both murine model and human tissues, and found that the frequency of CXCR4 expression increased with the progression of PanIN (31). Consistent with this report, our genetically engineered mouse models clearly demonstrated that both the number and grade of the PanIN lesions were significantly lower in *Cxcr4* KO mice compared with *Cxcr4* WT mice. These findings suggest that CXCR4 plays an important role in the formation and progression of PanIN, namely the initiation of PDAC.

On the basis of these results, we next compared the rate of pancreatic tumor formation between *KPC-Cxcr4-WT* and *KPC-Cxcr4-KO* mice, expecting that tumor formation would be suppressed in *KPC-Cxcr4-KO* mice. CXCR4 is expressed in many types of human cancers including PDAC, and strong CXCR4 expression in tumors is reportedly associated with a lower survival rate (32). Indeed, CXCR4 is reported to promote cancer progression through an EMT and subsequent metastasis (17, 33, 34). Furthermore, Feig and colleagues reported that targeting CXCL12 from stromal cells promotes T-cell infiltration and improves the effects of anti–PD-L1 immunotherapy on PDACs (35). Chen and colleagues reported that blocking of CXCL12/CXCR4 caused reduction of tumor fibrosis, alleviates immunosuppression, and significantly enhances the effect of immune checkpoint blockers in metastatic breast cancer (36). Therefore, many studies have investigated CXCR4 as a cancer therapeutic target, for example, neutralizing antibody immunotherapy in colorectal cancer (37), polymeric anti-CXCR4 drug AMD3100 nanoparticles for small interference RNA delivery in melanoma (38), etc. Quite surprisingly, however, our analysis of the PDAC mouse model revealed that *Cxcr4* KO did not reduce the tumor frequency, and rather increased the tumor size while precancerous lesion PanIN was reduced in KPC-Cxcr4-KO mice. This reason is unclear; however, one possibility is that pancreatic cancer of *KPC-Cxcr4-KO* mice is not generated from canonical PanIN to cancer cascade but from other precancerous cells. Another possibility is that CXCR4 is essential for the maintaining of PanIN's apparent form but not so involved in its carcinogenic function but in its differentiation form.

Furthermore, *Cxcr4* KO changed the tumor phenotype to less of a desmoplastic reaction with a higher density of tumor cells and scant fibroblasts and collagens. *In vitro* analysis revealed that *Cxcr4* KO tumor cells had a more proliferative and more active migration phenotype with more mesenchymal features, whereas *in vivo* analysis showed less metastatic phenotype. These contrasting results indicate a difference between the effects of *Cxcr4* KO on the tumor cells themselves and on tumor cell–organ interactions. Cxcl12/Cxcr4 may play a role in the organ microenvironment, including intravascular invasion, chemotaxis, adhesion, or extravasation required for metastasis, as previously reported (18, 39, 40). Our analysis is the first report of conditional-KO of *Cxcr4* in a PDAC mouse model, and may represent a much truer phenotype than the previous analysis using *Cxcr4* knockdown or inhibitors. *Cxcr4* KO could directly alter the characteristics of tumor cells. Indeed, IHC and microarray analysis revealed reduced activation of MAPK/ERK pathway downstream of CXCR4 signaling in tumor cells from *KPC-Cxcr4-KO* mice (41, 42). It is known that, in Kras-driven cancer model, suppression of Kras/MAPK signaling activates alternative pathways for cancer proliferation and survival (43, 44). These observations suggest that knockout of *Cxcr4* affected the canonical MAPK/ERK pathway and contributed to the acquisition of a Kras-independent and EMT phenotype, leading to the rather autonomous proliferations of KPC-Cxcr4-KO tumor cells that do not require stromal cells (45). Another possibility is that changes in the tumor microenvironment, such as the diminished desmoplastic reaction by *Cxcr4* KO may reversely affect the characteristics of tumor cells.

To elucidate the mechanisms of the changing tumor phenotype in *KPC-Cxcr4-KO* mice, we focused on the interaction between tumor cells and the tumor microenvironment, including fibroblasts. CXCR4 and its ligand CXCL12 are key factors in the cancer microenvironment that induce activation of fibroblasts and angiogenesis in cancer tissues (18, 46, 47). To clarify the mechanisms of the undifferentiated and fewer desmoplastic characteristics in *Cxcr4* KO tumors, we focused on cancer cell–fibroblast interactions. Although the limitation of the *in vitro* 2D system need to be considered, we found that myofibroblasts, but not cancer cells, produce and secrete Cxcl12 and induce tumor cell migration toward myofibroblasts in a Cxcl12/Cxcr4 signaling–dependent manner. On the other hand, *Cxcr4* KO tumor cells were not affected by myofibroblasts and appeared to survive more independently from mesenchymal cells. Several studies have suggested that myofibroblasts surrounding cancer cells have a tumor-promoting function in solid tumors via angiogenesis (48) and protect against anticancer drug exposure (49). On the other hand, some studies report that depletion of myofibroblasts exacerbates the pancreatic tumor phenotype (7, 50). Rhim and colleagues reported that removal of myofibroblasts surrounding pancreatic cancer tissues weakened the invasive ability of the tumor and changed the tumor phenotype to undifferentiated carcinoma (7). Collison and colleagues reported that human pancreatic cancer with few fibroblasts demonstrate Kras-independent phenotype and poor prognosis (45). Taking these previous findings into consideration, the characteristic phenotype of undifferentiated features and less desmoplasia in *Cxcr4* KO tumors could be due to the lack of interaction between tumor cells and myofibroblasts, and the aggressive proliferation/invasion trait may increase independent of the Cxcl12/Cxcr4 axis.

Finally, we used IHC to evaluate CXCR4 protein expression in surgically resected specimens of human pancreatic cancer. Most of cancer cells in PDAC with a characteristic desmoplastic reaction strongly expressed CXCR4. Surprisingly, in human pancreatic undifferentiated carcinoma without a desmoplastic reaction, the cancer cells express vimentin but not CXCR4, which is quite similar to the phenotype of *Cxcr4* KO mice. These findings indicated that Cxcr4 KO mice can be considered as a mouse model correlating with human undifferentiated cancer and that CXCR4 may also be associated with the desmoplastic reaction in human PDAC.

In summary, this study is the first to analyze the role of CXCR4 in the formation of PDAC using *Cxcr4* conditional-KO mice. We provide evidence that the CXCR12/CXCR4 axis plays an essential role in the development of the characteristic desmoplastic reaction in PDAC and loss of *CXCR4* induces phenotype alterations to undifferentiated carcinoma without a desmoplastic reaction. The current study will reveal that CXCR4 is one of the key regulator of desmoplastic reaction in PDAC and open the way for new therapeutic approaches to overcome the chemoresistance in patients with PDAC.

Disclosure of Potential Conflicts of Interest

No potential conflicts of interest were disclosed.

Authors' Contributions

T. Morita: Conceptualization, resources, data curation, formal analysis, validation, investigation, visualization, methodology, writing-original draft, writing-review and editing. **Y. Kodama:** Conceptualization, supervision, funding acquisition. **M. Shiokawa:** Investigation. **K. Kuriyama:** Investigation. **S. Marui:** Investigation. **T. Kuwada:** Investigation. **Y. Sogabe:** Investigation. **T. Matsumori:** Investigation. **N. Kakiuchi:** Investigation. **T. Tomono:** Investigation. **A. Mima:** Investigation. **T. Ueda:** Investigation. **M. Tsuda:** Investigation. **Y. Yamauchi:** Investigation. **Y. Nishikawa:** Investigation. **Y. Sakuma:** Investigation. **Y. Ota:** Investigation. **T. Maruno:** Investigation. **N. Uza:** Supervision, investigation. **T. Nagasawa:** Resources. **T. Chiba:** Supervision. **H. Seno:** Supervision.

Acknowledgments

This work was supported by the Japan Society for the Promotion of Science (JSPS) and the Ministry of Education, Culture, Sports, Science and Technology (MEXT) KAKENHI Grant Numbers JP15J05143, JP17H06803, and JP16K09395. We wish to thank Yuta Kawamata for excellent technical support.

The costs of publication of this article were defrayed in part by the payment of page charges. This article must therefore be hereby marked *advertisement* in accordance with 18 U.S.C. Section 1734 solely to indicate this fact.

Received September 2, 2019; revised February 6, 2020; accepted June 25, 2020; published first June 30, 2020.

References

1. Bardeesy N, DePinho RA. Pancreatic cancer biology and genetics. Nat Rev Cancer 2002;2:897–909.
2. Jemal A, Bray F, Center MM, Ferlay J, Ward E, Forman D. Global cancer statistics. CA Cancer J Clin 2011;61:69–90.
3. Hruban RH, Adsay NV, Albores-Saavedra J, Compton C, Garrett ES, Goodman SN, et al. Pancreatic intraepithelial neoplasia: a new nomenclature and classification system for pancreatic duct lesions. Am J Surg Pathol 2001;25:579–86.
4. Stanger BZ, Hebrok M. Control of cell identity in pancreas development and regeneration. Gastroenterology 2013;144:1170–9.
5. Pandol S, Edderkaoui M, Gukovsky I, Lugea A, Gukovskaya A. Desmoplasia of pancreatic ductal adenocarcinoma. Clin Gastroenterol Hepatol 2009;7: S44–7.
6. Bailey JM, Swanson BJ, Hamada T, Eggers JP, Singh PK, Caffery T, et al. Sonic hedgehog promotes desmoplasia in pancreatic cancer. Clin Cancer Res 2008;14: 5995–6004.
7. Rhim AD, Oberstein PE, Thomas DH, Mirek ET, Palermo CF, Sastra SA, et al. Stromal elements act to restrain, rather than support, pancreatic ductal adenocarcinoma. Cancer Cell 2014;25:735–47.
8. Provenzano PP, Cuevas C, Chang AE, Goel VK, Von Hoff DD, Hingorani SR. Enzymatic targeting of the stroma ablates physical barriers to treatment of pancreatic ductal adenocarcinoma. Cancer Cell 2012;21:418–29.
9. Tanaka M, Fukayama M, Fukushima N. Undifferentiated carcinoma of the pancreas with/without osteoclast-like giant cells. Pathol Case Rev 2010;15:210–4.
10. Tschang TP, Garza-Garza R, Kissane JM. Pleomorphic carcinoma of the pancreas: an analysis of 15 cases. Cancer 1977;39:2114–26.
11. Tokoyoda K, Egawa T, Sugiyama T, Choi BI, Nagasawa T. Cellular niches controlling B lymphocyte behavior within bone marrow during development. Immunity 2004;20:707–18.
12. Domanska UM, Kruizinga RC, Nagengast WB, Timmer-Bosscha H, Huls G, de Vries EG, et al. A review on CXCR4/CXCL12 axis in oncology: no place to hide. Eur J Cancer 2013;49:219–30.
13. Wang Z, Ma Q, Liu Q, Yu H, Zhao L, Shen S, et al. Blockade of SDF-1/CXCR4 signalling inhibits pancreatic cancer progression in vitro via inactivation of canonical Wnt pathway. Br J Cancer 2008;99:1695–703.
14. Wu H, Zhu L, Zhang H, Shi X, Zhang L, Wang W, et al. Coexpression of EGFR and CXCR4 predicts poor prognosis in resected pancreatic ductal adenocarcinoma. PLoS One 2015;10:e0116803.
15. Bhagat TD, Von Ahrens D, Dawlaty M, Zou Y, Baddour J, Achreja A, et al. Lactate-mediated epigenetic reprogramming regulates formation of human pancreatic cancer-associated fibroblasts. Elife 2019;8:e50663.
16. Heinrich EL, Lee W, Lu J, Lowy AM, Kim J. Chemokine CXCL12 activates dual CXCR4 and CXCR7-mediated signaling pathways in pancreatic cancer cells. J Transl Med 2012;10:68.
17. Muller A, Homey B, Soto H, Ge N, Catron D, Buchanan ME, et al. Involvement of chemokine receptors in breast cancer metastasis. Nature 2001;410:50–6.
18. Orimo A, Gupta PB, Sgroi DC, Arenzana-Seisdedos F, Delaunay T, Naeem R, et al. Stromal fibroblasts present in invasive human breast carcinomas promote tumor growth and angiogenesis through elevated SDF-1/CXCL12 secretion. Cell 2005;121:335–48.
19. Sugiyama T, Kohara H, Noda M, Nagasawa T. Maintenance of the hematopoietic stem cell pool by CXCL12-CXCR4 chemokine signaling in bone marrow stromal cell niches. Immunity 2006;25:977–88.
20. Gu G, Dubauskaite J, Melton DA. Direct evidence for the pancreatic lineage: NGN3+ cells are islet progenitors and are distinct from duct progenitors. Development 2002;129:2447–57.
21. Jackson EL, Willis N, Mercer K, Bronson RT, Crowley D, Montoya R, et al. Analysis of lung tumor initiation and progression using conditional expression of oncogenic K-ras. Genes Dev 2001;15:3243–8.
22. Olive KP, Tuveson DA, Ruhe ZC, Yin B, Willis NA, Bronson RT, et al. Mutant p53 gain of function in two mouse models of Li-Fraumeni syndrome. Cell 2004; 119:847–60.
23. Nishikawa Y, Kodama Y, Shiokawa M, Matsumori T, Marui S, Kuriyama K, et al. Hes1 plays an essential role in Kras-driven pancreatic tumorigenesis. Oncogene 2019;38:4283–96.
24. Herreros-Villanueva M, Hijona E, Cosme A, Bujanda L. Mouse models of pancreatic cancer. World J Gastroenterol 2012;18:1286–94.
25. Grant AG, Duke D, Hermon-Taylor J. Establishment and characterization of primary human pancreatic carcinoma in continuous cell culture and in nude mice. Br J Cancer 1979;39:143–51.
26. Burger JA, Kipps TJ. CXCR4: a key receptor in the crosstalk between tumor cells and their microenvironment. Blood 2006;107:1761–7.
27. Liu P, Long P, Huang Y, Sun F, Wang Z. CXCL12/CXCR4 axis induces proliferation and invasion in human endometrial cancer. Am J Transl Res 2016;8:1719–29.
28. Tachibana K, Hirota S, Iizasa H, Yoshida H, Kawabata K, Kataoka Y, et al. The chemokine receptor CXCR4 is essential for vascularization of the gastrointestinal tract. Nature 1998;393:591–4.
29. Zou Y-R, Kottmann AH, Kuroda M, Taniuchi I, Littman DR. Function of the chemokine receptor CXCR4 in haematopoiesis and in cerebellar development. Nature 1998;393:595–9.

Published OnlineFirst June 30, 2020; DOI: 10.1158/0008-5472.CAN-19-2745

30. Katsumoto K, Kume S. The role of CXCL12-CXCR4 signaling pathway in pancreatic development. Theranostics 2013;3:11–7.
31. Thomas RM, Kim J, Revelo-Penafiel MP, Angel R, Dawson DW, Lowy AM. The chemokine receptor CXCR4 is expressed in pancreatic intraepithelial neoplasia. Gut 2008;57:1555–60.
32. Schimanski CC, Wolfert F, Gockel I, Junginger T, Galle PR, Moehler M. Expression of chemokine receptor CXCR4 correlates with progression of pancreatic cancer. J Clin Oncol 2006;24:14018-.
33. Schimanski CC, Bahre R, Gockel I, Muller A, Frerichs K, Horner V, et al. Dissemination of hepatocellular carcinoma is mediated via chemokine receptor CXCR4. Br J Cancer 2006;95:210–7.
34. Lv B, Yang X, Lv S, Wang L, Fan K, Shi R, et al. CXCR4 signaling induced epithelial-mesenchymal transition by PI3K/AKT and ERK pathways in glioblastoma. Mol Neurobiol 2015;52:1263–8.
35. Feig C, Jones JO, Kraman M, Wells RJ, Deonarine A, Chan DS, et al. Targeting CXCL12 from FAP-expressing carcinoma-associated fibroblasts synergizes with anti-PD-L1 immunotherapy in pancreatic cancer. Proc Natl Acad Sci U S A 2013;110:20212–7.
36. Chen IX, Chauhan VP, Posada J, Ng MR, Wu MW, Adstamongkonkul P, et al. Blocking CXCR4 alleviates desmoplasia, increases T-lymphocyte infiltration, and improves immunotherapy in metastatic breast cancer. Proc Natl Acad Sci U S A 2019;116:4558–66.
37. Ottaiano A, di Palma A, Napolitano M, Pisano C, Pignata S, Tatangelo F, et al. Inhibitory effects of anti-CXCR4 antibodies on human colon cancer cells. Cancer Immunol Immunother 2005;54:781–91.
38. Wang Y, Li J, Oupicky D. Polymeric Plerixafor: effect of PEGylation on CXCR4 antagonism, cancer cell invasion, and DNA transfection. Pharm Res 2014;31:3538–48.
39. Hartmann TN, Burger JA, Glodek A, Fujii N, Burger M. CXCR4 chemokine receptor and integrin signaling co-operate in mediating adhesion and chemoresistance in small cell lung cancer (SCLC) cells. Oncogene 2005;24:4462–71.
40. Meads MB, Hazlehurst LA, Dalton WS. The bone marrow microenvironment as a tumor sanctuary and contributor to drug resistance. Clin Cancer Res 2008;14:2519–26.
41. Burger M, Glodek A, Hartmann T, Schmitt-Graff A, Silberstein LE, Fujii N, et al. Functional expression of CXCR4 (CD184) on small-cell lung cancer cells mediates migration, integrin activation, and adhesion to stromal cells. Oncogene 2003;22:8093–101.
42. Zhao HB, Tang CL, Hou YL, Xue LR, Li MQ, Du MR, et al. CXCL12/CXCR4 axis triggers the activation of EGF receptor and ERK signaling pathway in CsA-induced proliferation of human trophoblast cells. PLoS One 2012;7:e38375.
43. Singh A, Greninger P, Rhodes D, Koopman L, Violette S, Bardeesy N, et al. A gene expression signature associated with "K-Ras addiction" reveals regulators of EMT and tumor cell survival. Cancer Cell 2009;15:489–500.
44. Shao DD, Xue W, Krall EB, Bhutkar A, Piccioni F, Wang X, et al. KRAS and YAP1 converge to regulate EMT and tumor survival. Cell 2014;158:171–84.
45. Collisson EA, Sadanandam A, Olson P, Gibb WJ, Truitt M, Gu S, et al. Subtypes of pancreatic ductal adenocarcinoma and their differing responses to therapy. Nat Med 2011;17:500–3.
46. Burger JA, Peled A. CXCR4 antagonists: targeting the microenvironment in leukemia and other cancers. Leukemia 2009;23:43–52.
47. Liang Z, Brooks J, Willard M, Liang K, Yoon Y, Kang S, et al. CXCR4/CXCL12 axis promotes VEGF-mediated tumor angiogenesis through Akt signaling pathway. Biochem Biophys Res Commun 2007;359:716–22.
48. Vong S, Kalluri R. The role of stromal myofibroblast and extracellular matrix in tumor angiogenesis. Genes Cancer 2011;2:1139–45.
49. Hazlehurst LA, Landowski TH, Dalton WS. Role of the tumor microenvironment in mediating de novo resistance to drugs and physiological mediators of cell death. Oncogene 2003;22:7396–402.
50. Ozdemir BC, Pentcheva-Hoang T, Carstens JL, Zheng X, Wu CC, Simpson TR, et al. Depletion of carcinoma-associated fibroblasts and fibrosis induces immunosuppression and accelerates pancreas cancer with reduced survival. Cancer Cell 2014;25:719–34.

Cancer Research
The Journal of Cancer Research (1916–1930) | The American Journal of Cancer (1931–1940)

AACR American Association for Cancer Research

CXCR4 in Tumor Epithelial Cells Mediates Desmoplastic Reaction in Pancreatic Ductal Adenocarcinoma

Toshihiro Morita, Yuzo Kodama, Masahiro Shiokawa, et al.

Cancer Res 2020;80:4058-4070. Published OnlineFirst June 30, 2020.